

Flow Resistance and Structures in Viscoelastic Channel Flows at Low Re

Boyang Qin¹, Paul F. Salipante,² Steven D. Hudson,² and Paulo E. Arratia¹

¹*Department of Mechanical Engineering & Applied Mechanics, University of Pennsylvania, Philadelphia, Pennsylvania 19104, USA*

²*Polymers & Complex Fluids Group, National Institute of Standards and Technology, Gaithersburg, Maryland 20899, USA*

(Received 2 July 2018; revised manuscript received 13 January 2019)

The flow of viscoelastic fluids in channels and pipes remains poorly understood, particularly at low Reynolds numbers. Here, we investigate the flow of polymeric solutions in straight channels using pressure measurements and particle tracking. The flow friction factor f_η versus flow rate exhibits two regimes: a transitional regime marked by rapid increase in drag, and a turbulentlike regime characterized by a sudden decrease in drag and a weak dependence on flow rate. Lagrangian trajectories show finite transverse modulations not seen in Newtonian fluids. These curvature perturbations far downstream can generate sufficient hoop stresses to sustain the flow instabilities in the parallel shear flow.

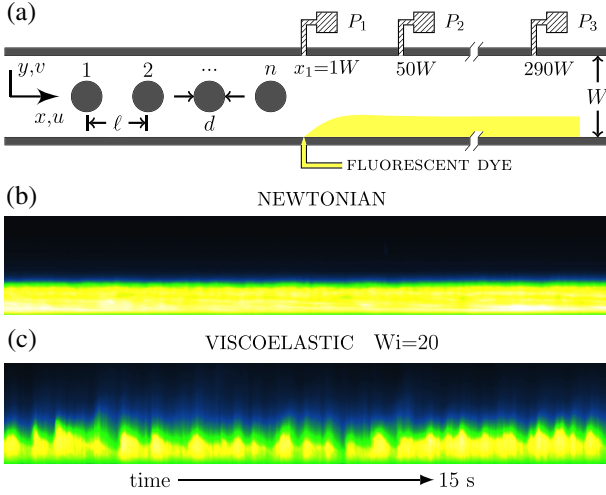
DOI: 10.1103/PhysRevLett.123.194501

Fluids containing polymers are found in everyday life (e.g., foods and cosmetics) and in technology spanning the oil, pharmaceutical, and chemical industries. A marked characteristic of polymeric fluids is that they often exhibit non-Newtonian flow behavior such as viscoelasticity [1,2]. Mechanical (elastic) stresses in such fluids are history dependent and develop with timescale λ , which is proportional to the time needed for a single polymer molecule to relax to its equilibrium state in dilute solutions. These stresses grow nonlinearly with shear rate and can dramatically change the flow behavior [1,2]. For example, the presence of the polymer in turbulent pipe flows can suppress eddies and leads to large reduction in flow friction [3,4]. At low Reynolds numbers (Re), where inertia is negligible, elastic stresses can lead to flow instabilities not found in ordinary fluids like water [5–12]. They can also exhibit a new type of disordered flow—elastic turbulence—a turbulentlike regime existing far below the dissipation scale [13–16].

Recently, there has been mounting evidence that the flow of viscoelastic polymeric solutions in pipe and channel flows is nonlinearly unstable and undergoes a subcritical instability at sufficiently high flow rates even at low Re [12,17–22]. We note that this nonlinear elastic instability is different from the linear instability found in highly shear-thinning fluids [23–26]; the base flow of the former is stable while the latter is unstable. Each is important in its own right. Theoretical investigations using Oldroyd-B-type model and nonlinear perturbation analysis show that a subcritical bifurcation can arise from linearly stable base states [17,19,20,27], while nonmodal stability analysis predicts transient growth of perturbation [28–30]. Subsequent experiments in small pipes found unusually large velocity fluctuations that are activated at many timescales [21], as

well as hysteretic behavior [18]. More recently, experiments in a long microchannel using a linear array of cylinders as a way to perturb the (viscoelastic) flow showed an abrupt transition to irregular flow and that the velocity fluctuations are long lived [12,22]. The unstable flow exhibits features of Newtonian turbulence such as power-law behavior in velocity spectra, intermittency flow statistics, and irregular structures in the streamwise velocity fluctuation [22]. Taken together, these results show that polymeric solutions flowing in straight channels can undergo a subcritical transition—a sudden onset of sustained velocity fluctuations above a perturbation threshold and a critical flow rate. This scenario is akin to the transition from laminar to turbulent flow of Newtonian fluids in pipe flows [31,32]. The main distinction is that the instability is caused by the nonlinear elastic stresses and not inertia. Unlike the Newtonian pipe turbulence, however, little is known about the basic structures organizing the instability and the law of resistance (i.e., pressure loss due to friction) as the flow transitions from a stable to an unstable state.

In this Letter, we investigate the flow of polymeric solutions in a straight microchannel at low Re using pressure measurements and particle tracking methods. Pressure measurements show that the flow resistance increases relative to the stable viscoelastic base flow, following the transition from a laminar to “turbulentlike” state, cf. Fig. 1(c). This behavior is analogous to Newtonian turbulence where the friction factor increases as the flow transitions from laminar to turbulent except that here the governing parameter is the Weissenberg number (Wi), defined as the product of the fluid relaxation time λ and the flow shear rate $\dot{\gamma}$. The rise in flow resistance is related to enhanced elastic stresses and suggests flow patterns not seen in the (viscoelastic) laminar regime. We find that, far



F1:1 FIG. 1. (a) Schematic of the microchannel, showing location of
 F1:2 pressure sensors and the dye injection scheme. [(b) and (c)]
 F1:3 Spacetime dye patterns for $n = 15$ and $x = 200$ W in the parallel
 F1:4 shear region, (c) viscoelastic fluid at $Wi = 20$, and (b) the
 F1:5 Newtonian case at identical flow rate.

85 downstream from the initial perturbation, tracer particles
 86 follow wavy trajectories with spanwise modulation not
 87 found in the stable unperturbed flow (cf. Fig. 5). We believe
 88 that the increase in flow resistance is connected to the
 89 appearances of these wavy particle motions. A friction factor
 90 scaling (i.e., flow resistance vs pressure drop) for visco-
 91 elastic channel flows is proposed to capture this increase
 92 in drag.

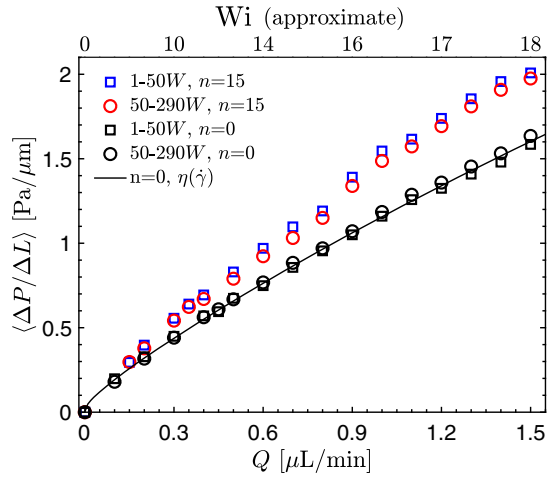
93 Experiments are conducted using a straight microchan-
 94 nel with equal width and depth ($W = D = 100 \mu\text{m}$),
 95 fabricated using standard soft-lithography methods. The
 96 device schematic is shown in Fig. 1(a). The channel length
 97 is much larger than its width $L/W = 330$ and is divided
 98 into two regions. The first region consists of a linear array
 99 of fifteen cylinders ($n = 15$) that extends for 30 W, with
 100 the last cylinder located at $x = 0$. The diameter of the cylinder
 101 is $d = 0.5$ W and the center to center separation is
 102 $\ell = 2$ W. An unperturbed control case with no cylinders
 103 ($n = 0$) is used as the linearly stable viscoelastic case. The
 104 second region follows the array of cylinders and consists of
 105 a long parallel shear flow 300 W in length. To measure
 106 pressure signals, sensors are placed at three locations in
 107 the parallel shear region, $x_1 = 1$ W, $x_2 = 50$ W, $x_3 =$
 108 290 W [see Fig. 1(a)]. The pressure drop per length $p_1(t) =$
 109 $(P_1 - P_2)/(x_2 - x_1)$ and $p_2(t) = (P_2 - P_3)/(x_3 - x_2)$ is
 110 recorded at 5 ms resolution for over 2 hours.

111 The main polymeric solution is prepared by adding
 112 300 ppm of polyacrylamide (PAA, 18×10^6 MW) to a
 113 viscous Newtonian solvent (90% by mass glycerol aqueous
 114 solution); the PAA polymer overlap concentration c^*
 115 is 350 ppm [33] and $c/c^* = 0.86$. This weakly shear-
 116 thinning polymeric solution has a nearly constant viscosity
 117 of around $\eta = 300$ mPa s. The Newtonian solvent has

constant viscosity of 220 mPa s and is also used for
 comparison. Throughout our experiment, the Reynolds
 number is kept below 0.01 , where $Re = \rho UH/\eta$, U is the
 mean centerline velocity, H is the channel half-width, and ρ
 is the fluid density. We characterize the strength of the elastic
 stresses compared to viscous stresses by the Weissenberg
 number [7], defined here as $Wi(\dot{\gamma}) = N_1(\dot{\gamma})/2\dot{\gamma}\eta(\dot{\gamma})$, where
 $\dot{\gamma} = U/H$ is the shear rate and N_1 is the first normal stress
 difference (see Supplemental Material [34] for fluid rheol-
 ogy and residence time).

We begin by investigating the flow patterns formed when
 a stream of experimental fluid with added fluorescent dye is
 injected at $x = 1$ W after the last post. The dye spreading
 and patterns are then visualized far downstream in the
 parallel shear region, 200 W downstream from the last post.
 Figure 1 shows the spatiotemporal profile of the dye
 intensity along the device's cross section (y) for a channel
 containing 15 posts ($n = 15$) for Newtonian [Fig. 1(b)] and
 viscoelastic [Fig. 1(c)] fluids. For the Newtonian case, the
 profile shows typical laminar dye layer with minimal dye
 penetration into the undyed stream, except for diffusion.
 (Similar behavior is observed with viscoelastic fluids for the
 $n = 0$ case.) A different dye pattern is observed when the
 Newtonian fluid is replaced by the polymeric solution under
 the same conditions. The viscoelastic case, shown in
 Fig. 1(c) at $Wi \approx 20$, shows irregular flow patterns with
 spikes of dye penetration into the undyed fluid stream. The
 flow structure of streamwise velocity showed similar devel-
 opment downstream (Supplemental Material [34]). These
 fluctuations in time suggest flow modulations normal to the
 mean flow. In fact, we show later that particle trajectories
 exhibit wavy coherent motions in the parallel shear region.

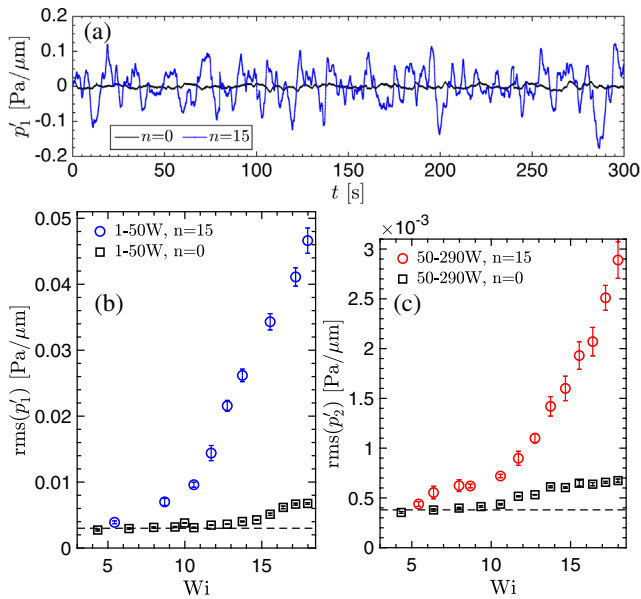
As mentioned before, little is known about elastic
 turbulence in channel flows. Importantly, there is no known
 law of resistance for such flows. Here, we observe a new
 friction factor scaling for long chain polymeric solutions
 with weak shear thinning in straight channel flows. Figure 2
 shows the mean pressure drop per length signals p_1 , p_2 for
 viscoelastic fluids for $n = 0$ and 15 cases as a function of
 flow rate Q and Wi . We note that the statistical mean of the
 reported signals measures the aggregate flow resistance
 encountered to sustain a constant mass flow rate. As
 expected, the pressure drop or flow resistance increases
 with flow rate and Wi . The pressure drop for the $n = 0$ case
 slightly deviates from the Newtonian case (i.e., $\Delta P \sim Q$)
 due to mild shear thinning in fluid viscosity. These effects
 can be accounted for by estimating the pressure drop using
 wall shear rate and corresponding viscosity $\eta(\dot{\gamma})$ measured
 using a cone-and-plate rheometer, as shown by the solid
 line in Fig. 2. No significant difference is found between p_1
 and p_2 for the $n = 0$ case as expected, since entrance
 effects are minimized by using a tapered inlet that generates
 minor disturbance relative to that of the cylinder array. For
 $n = 15$, we find a clear increase in pressure drop relative to
 the $n = 0$ case; the two pressure segments p_1 and p_2 show



F2:1 FIG. 2. Pressure drop per unit length as a function of flow rate
 F2:2 Q and Wi for $n = 15$ and $n = 0$ cases. The solid line represents
 F2:3 estimation using wall shear rates and viscosity from rheology
 F2:4 measurements. Error bars are less than marker size and not
 F2:5 shown here.

173 little to no difference. This increase in flow resistance
 174 cannot be explained by solely shear-thinning effects and is
 175 related to the development of additional elastic stresses in
 176 the flow as the Wi is increased. It also indicates that more
 177 energy is necessary to keep the same flow rate compared to
 178 a stable viscoelastic channel flow.

179 The increase in flow resistance is closely associated with
 180 the onset of pressure fluctuations (Fig. 3). Figure 3(a)

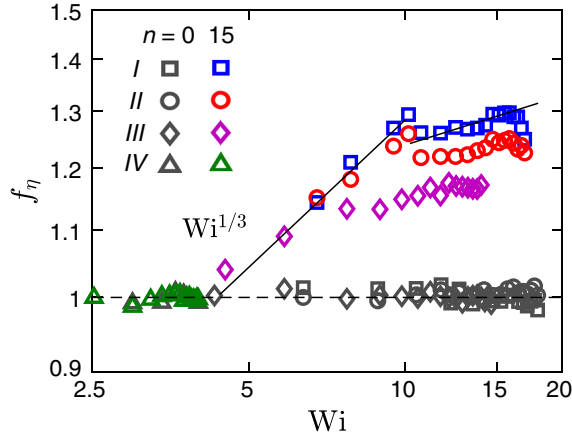


F3:1 FIG. 3. (a) Pressure gradient signal $p'_1(t)$ for the $n = 15$ case,
 F3:2 compared with the unperturbed $n = 0$ case, $Wi = 18$. [(b) and
 F3:3 (c)] Root-mean-square (rms) fluctuations versus Wi for $n = 0$
 F3:4 and 15 , (b) p'_1 , and (c) p'_2 . The dashed line is the average level
 F3:5 for Newtonian fluid, experimentally found to be constant for
 F3:6 increasing Q .

181 shows sample time records of pressure fluctuations $p'_1(t)$ 181
 182 for viscoelastic fluids at $Wi = 18$ in devices with $n = 0$ 182
 183 (black) and 15 (blue). We observe a clear increase in the 183
 184 pressure fluctuations far downstream the cylinders once they 184
 185 are introduced in the flow. Figures 3(a) and 3(b) show 185
 186 rms values of the pressure fluctuations of the p'_1 and p'_2 186
 187 segments, respectively, as a function of Wi for the $n = 15$ 187
 188 and $n = 0$ cases. For the $n = 0$ case, pressure fluctuations 188
 189 remain relatively small and nearly independent of Wi ; the 189
 190 small increase in pressure fluctuation at the higher values of 190
 191 Wi may be due to entrance effects. We find that for both 191
 192 segments, p'_1 and p'_2 , the rms values show significant 192
 193 departure from the stable $n = 0$ case and a marked 193
 194 increased with increasing Wi . The values of the rms(p'_1) 194
 195 and rms(p'_2) start to depart from the $n = 0$ trend at $Wi \approx 5$ 195
 196 and grow weakly until $Wi \approx 9$. This is followed by a much 196
 197 steeper growth for $Wi \gtrsim 9$. This trend in pressure fluc- 197
 198 tuation measurements agrees relatively well with measure- 198
 199 ments of velocity fluctuations, for the $n = 15$ case, which 199
 200 established that the linear instability associated with the 200
 201 flow around the upstream cylinders occurs at $Wi \approx 4$ and 201
 202 the onset of subcritical instability occurs at $Wi \approx 9$ [12,22]. 202

203 Since pressure data are now available, one can 203
 204 investigate the law of flow resistance for viscoelastic 204
 205 channel flows as a function of Wi . This is analogous to 205
 206 measuring the Darcy friction factor for Newtonian pipe 206
 207 flows as a function of Re [37], traditionally defined as 207
 208 $(\Delta P / \Delta L) / (\rho U^2 / 2W)$. For small geometry variations (e.g., 208
 209 smooth pipes), the friction factor f is solely a function of 209
 210 Re . In what follows, we propose that there is an analogous 210
 211 law of resistance for viscoelastic channel flows controlled 211
 212 by Wi . Since fluid inertia in our experiments is negligible 212
 213 ($Re \lesssim 10^{-3}$), we propose to scale the pressure drop by the 213
 214 viscous stresses across the channel and define a viscous 214
 215 friction factor f_η as $(\Delta P / \Delta L) / (c\eta_w \dot{\gamma}_w / W)$, where $\dot{\gamma}_w$ is the 215
 216 wall shear rate, η_w is the corresponding viscosity, and 216
 217 geometry factor $c \approx 4$ for square duct (Supplemental 217
 218 Material [34]). 218

219 Figure 4 shows the friction factor f_η versus Wi for the 219
 220 main polymeric fluid, as well as two other fluids with 220
 221 different polymer concentrations and solvent viscosity (see 221
 222 [34]) in channels with $n = 0$ and 15 . For $n = 0$, the friction 222
 223 factor is independent of Wi , indicating that the flow 223
 224 resistance is purely governed by viscous drag well 224
 225 accounted for by the normalization. For $n = 15$, however, 225
 226 we observe an increase in flow resistance with $f_\eta \sim Wi^{1/3}$ 226
 227 up to $Wi \approx 9$. Surprisingly, we find a second plateaulike 227
 228 regime for $Wi \gtrsim 9$ in which a sudden decrease in f_η is 228
 229 observed followed by a weak dependence on Wi , valid 229
 230 before polymer finite extensibility occurs at $Wi \gtrsim 16$. This 230
 231 relative decrease in drag seems to suggest the emergence of 231
 232 a new flow state. The data in Fig. 4 suggest that the initial 232
 233 $f_\eta \sim Wi^{1/3}$ regime is likely a transitional state leading to a 233
 234 fully turbulentlike state. Similar to Newtonian pipe flows, a 234

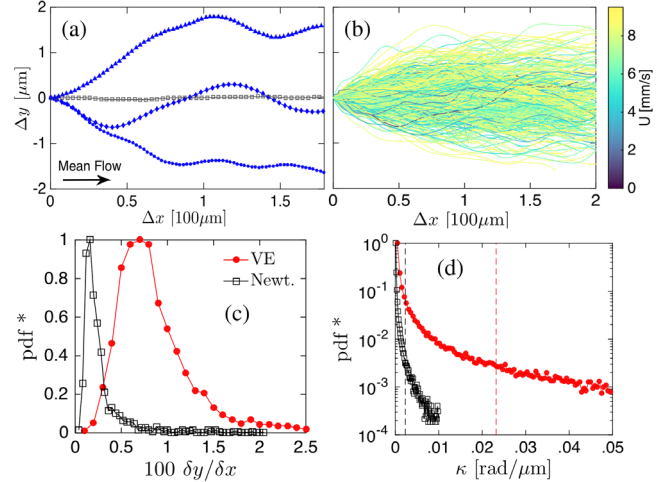


F4:1 FIG. 4. Viscous friction factor f_η as a function of Wi for $n = 0$
 F4:2 and 15 with four cases and types of polymeric fluids. Case I:
 F4:3 300 ppm PAA 90% glycerol, 0–50 W, II: 50–290 W, III: 250 ppm
 F4:4 PAA 90% glycerol, 0–290 W, IV: 100 ppm PAA 93% glycerol,
 F4:5 0–290 W.

235 sharp increase in drag occurs during the transition regime
 236 before the flow becomes fully turbulent. We note the $Wi^{1/3}$
 237 scaling observed here is lower than the $Wi^{1/2}$ scaling of
 238 injected power in the elastic turbulence of a swirling
 239 parallel plate system where the base flow is curved and
 240 linearly unstable [38].

241 Next, we investigate the structure of the viscoelastic flow
 242 for $n = 15$ and $Wi = 18$; this is the regime in which we
 243 expect highly irregular flow but quantifying the presence of
 244 flow structures has been difficult due to the weak spanwise
 245 velocity component relative to the mean shear [22]. To
 246 interrogate the flow with enough spatial and temporal
 247 resolution, we use a novel three-dimensional holographic
 248 particle tracking method [39,40]. The flow is seeded with
 249 tracers (1 μm diam at 0.001%) imaged under microscope
 250 and high speed camera (5000 fps). Using a coherent light
 251 source, particle positions are reconstructed from the light
 252 scattering field on the imaging plane (see [34]). The
 253 uncertainty in particle centroid is 30 nm for in-plane x ,
 254 y components. The measurement window is located at
 255 $x = 200 W$ in the parallel shear region and extends for
 256 2.5 W streamwise and 0.9 W spanwise.

257 Figure 5(a) shows sample particle trajectories for the
 258 Newtonian (grey) and viscoelastic (blue) fluids for the $n =$
 259 15 and $Wi = 18$. While the particle trajectory in the
 260 Newtonian case follows the mean flow with little lateral
 261 motion, particle trajectories in the viscoelastic fluid case
 262 display a relatively pronounced waviness and lateral move-
 263 ment. This is not isolated to a few particles and Fig. 5(b)
 264 shows the full extent of the spanwise spread for 2000
 265 such Lagrangian trajectories sampled uniformly in the
 266 channel. Such wavy structures underlie the irregular dye
 267 transport patterns seen in Fig. 1(c). We quantify these
 268 deviations from the base flow by calculating the normalized
 269 distribution (pdf*) of the ratio between transverse to



F5:1 FIG. 5. (a) Particle trajectories in the streamwise (x) and
 F5:2 spanwise (y) direction; blue lines represent the $n = 15$ visco-
 F5:3 elastic case at $Wi = 18$ and the gray line is Newtonian at identical
 F5:4 conditions. (b) Collection of trajectories colored by speed. Distributions of (c)
 F5:5 cumulative transverse to streamwise displacements and (d) trajectory
 F5:6 curvatures, where the dashed line represents population mean.
 F5:7

270 streamwise cumulative displacements [Fig. 5(c)] defined
 271 as $\delta y / \delta x = \sum |dy_i| / \sum |dx_i|$, where dy_i and dx_i are
 272 particle displacements between frames. The Newtonian
 273 data (black) show minimal transverse component and set
 274 the measurement noise level. Particles in the viscoelastic
 275 fluid, however, exhibit small but finite values of transverse
 276 velocity and a broader distribution of individual particle
 277 end-to-end displacement. These results indicate the pres-
 278 ence of spanwise structures in viscoelastic fluids in parallel
 279 shear flows. While these deviations from the base flow are
 280 small in absolute terms (2% of the streamwise component),
 281 even small deviations in the velocity fields in viscoelastic
 282 fluids can represent significant increase in elastic stresses
 283 due to the nonlinear relationship between stress and
 284 velocity [41,42].

285 Can these curved particle trajectories drive or maintain
 286 flow instabilities far downstream (200 W)? Figure 5(d)
 287 shows the distribution of particle path line curvatures at
 288 200 W for $Wi = 18$, $n = 15$. The trajectories have a mean
 289 curvature of $\mathcal{R}^{-1} \approx .023 \mu\text{m}^{-1}$, which is an order of
 290 magnitude larger than the Newtonian counterpart. Using
 291 N_1 data (see [34]), we compute the Pakdel-McKinley
 292 condition $[(\lambda U / \mathcal{R}) Wi]^{1/2}$ [43]. We find a value of approx-
 293 imately 7, which is sufficiently large to trigger flow
 294 instabilities. Similarly, we find that hoop stresses $N_1 / \mathcal{R} =$
 295 8 Pa/ μm are of the same order (or higher) than the viscous
 296 drag $\Delta P / \Delta L|_{n=0} = 2 \text{ Pa}/\mu\text{m}$. Hence additional pressure
 297 head is lost to overcome elastic stresses induced by the
 298 chaotic flow. These results suggest that weak but nontrivial
 299 streamline curvatures generate sufficient elastic stress
 300 fluctuations in the secondary flow direction to sustain flow
 301 instabilities far downstream.

302 In summary, we investigated the flow of viscoelastic
 303 fluids in a long, straight microchannel at low Re. This flow
 304 becomes unstable via a nonlinear subcritical instability at a
 305 critical Wi for finite amplitude perturbations [12]. Pressure
 306 measurements are used to establish the friction factor
 307 scaling for this flow (Fig. 4). We find two regimes: (i) a
 308 transitional regime $5 \lesssim Wi \lesssim 9$ in which the (viscous)
 309 friction factor $f_\eta \sim Wi^{1/3}$, and (ii) a turbulentlike regime
 310 $Wi \gtrsim 9$ in which a sudden reduction of f_η is observed
 311 followed by a weaker dependence on flow rate. The
 312 increase in drag (30%, cf. laminar flow) is accompanied
 313 by an increase in pressure fluctuation and development of
 314 elastic hoop stresses due to finite spanwise curvature
 315 perturbations, which we quantify using high-resolution
 316 holographic particle tracking. Unlike the Reynolds stress
 317 in classical turbulence, the extra flow resistance here stems
 318 from elastic hoop stresses induced by curvature perturba-
 319 tions. Furthermore, the various levels of increased resis-
 320 tance for different polymeric fluid may be controlled by the
 321 distribution of such curvatures. At intermediate Re, recent
 322 studies on elastoinertial turbulence (EIT) proposed a direct
 323 path to the classic drag reduction asymptote, bypassing
 324 Newtonian turbulence [44,45]. Whether a common insta-
 325 bility underlies these two states, elastic turbulence and EIT,
 326 remains an open question. Finally, our results provide
 327 strong evidence for the “instability upon an instability”
 328 mechanism proposed for the finite amplitude transition of
 329 viscoelastic fluids in parallel flows [19] and develop new
 330 insights into the flow of polymeric solutions in channels
 331 and pipes. Even small perturbations in the velocity field can
 332 lead to large changes in elastic stress and flow drag.

333 **1** We thank B. Thomases, A. Morozov, R. Poole, and M.
 334 Graham for fruitful discussions. P. E. A. acknowledges
 335 support from NSF Grant No. CBET-1336171 and S. D.
 336 H. thanks NIST-on-Chip funding.

339
 340 **2** [1] R. G. Larson, *The Structure and Rheology of Complex*
 341 *Fluids* (Oxford University Press, New York, 1999), Vol. 33.
 342 **3** [2] R. Bird, C. Curtiss, R. Armstrong, and O. Hassager,
 343 *Dynamics of Polymeric Liquids: Fluid Mechanics*, 2nd ed.
 344 (John Wiley & Sons, New York, 1987), Vol. 1.
 345 [3] P. S. Virk, *AIChE J.* **21**, 625 (1975).
 346 [4] C. M. White and M. G. Mungal, *Annu. Rev. Fluid Mech.* **40**,
 347 235 (2008).
 348 [5] S. Muller, R. Larson, and E. Shaqfeh, *Rheol. Acta* **28**, 499
 349 (1989).
 350 [6] R. G. Larson, E. S. G. Shaqfeh, and S. J. Muller, *J. Fluid*
 351 *Mech.* **218**, 573 (1990).
 352 [7] G. H. McKinley, R. C. Armstrong, and R. A. Brown, *Proc.*
 353 *R. Soc. A* **344**, 265 (1993).
 354 [8] A. Groisman and V. Steinberg, *Phys. Fluids* **10**, 2451
 355 (1998).
 356 [9] K. Arora, R. Sureshkumar, and B. Khomami, *J. Fluid Mech.*
 357 **108**, 209 (2002).

[10] P. E. Arratia, C. C. Thomas, J. Diorio, and J. P. Gollub, *Phys. Rev. Lett.* **96**, 144502 (2006). 358
 [11] R. J. Poole, M. A. Alves, and P. J. Oliveira, *Phys. Rev. Lett.* 359
99, 164503 (2007). 360
 [12] L. Pan, A. Morozov, C. Wagner, and P. E. Arratia, *Phys. 361*
Rev. Lett. **110**, 174502 (2013). 362
 [13] A. Groisman and V. Steinberg, *New J. Phys.* **6**, 29 (2004). 363
 [14] A. Groisman and V. Steinberg, *Nature (London)* **405**, 53 364
 (2000). 365
 [15] A. Groisman and V. Steinberg, *Nature (London)* **410**, 905 366
 (2001). 367
 [16] M. A. Fardin, D. Lopez, J. Croso, G. Grégoire, O. Cardoso, 368
 G. H. McKinley, and S. Lerouge, *Phys. Rev. Lett.* **104**, 369
 178303 (2010). 370
 [17] B. Meulenbroek, C. Storm, A. N. Morozov, and W. van 371
 Saarloos, *J. Fluid Mech.* **116**, 235 (2004). 372
 [18] B. Meulenbroek, C. Storm, V. Bertola, C. Wagner, D. Bonn, 373
 and W. van Saarloos, *Phys. Rev. Lett.* **90**, 024502 (2003). 374
 [19] A. N. Morozov and W. van Saarloos, *Phys. Rev. Lett.* **95**, 375
 024501 (2005). 376
 [20] A. N. Morozov and W. van Saarloos, *Phys. Rep.* **447**, 112 377
 (2007). 378
 [21] D. Bonn, F. Ingremeau, Y. Amarouchene, and H. Kellay, 379
Phys. Rev. E **84**, 045301(R) (2011). 380
 [22] B. Qin and P. E. Arratia, *Phys. Rev. Fluids* **2**, 083302 381
 (2017). 382
 [23] H. J. Wilson, M. Renardy, and Y. Renardy, *J. Fluid Mech.* 383
80, 251 (1999). 384
 [24] H. Bodiguel, J. Beaumont, A. Machado, L. Martinie, H. 385
 Kellay, and A. Colin, *Phys. Rev. Lett.* **114**, 028302 (2015). 386
 [25] R. Poole, *Phys. Rev. Fluids* **1**, 041301 (2016). 387
 [26] H. Barlow, E. Hemingway, A. Clarke, and S. Fielding, *J.* 388
Fluid Mech. **270**, 66 (2019). 389
 [27] A. Morozov and W. van Saarloos, *J. Stat. Phys.* **175**, 554 390
 (2019). 391
 [28] N. Hoda, M. R. Jovanovi, and S. Kumar, *J. Fluid Mech.* **601**, 392
 407 (2008). 393
 [29] M. R. Jovanovic and S. Kumar, *Phys. Fluids* **22**, 023101 394
 (2010). 395
 [30] M. R. Jovanovic and S. Kumar, *J. Fluid Mech.* **166**, 755 (2011). 396
 [31] O. Reynolds, *Phil. Trans. R. Soc. London* **35**, 84 (1883). 397
 [32] K. Avila, D. Moxey, A. de Lozar, M. Avila, D. Barkley, and 398
 B. Hof, *Science* **333**, 192 (2011). 399
 [33] E. Pelletier, C. Viebke, J. Meadows, and P. Williams, 400
Langmuir **19**, 559 (2003). 401
 [34] See Supplemental Material at [http://link.aps.org/](http://link.aps.org/supplemental/10.1103/PhysRevLett.000.000000) 402
[supplemental/10.1103/PhysRevLett.000.000000](http://link.aps.org/supplemental/10.1103/PhysRevLett.000.000000) for details 403
 on rheology and experimental methods, which includes 404
 Refs. [35,36]. **4** 405
 [35] L. Pan and P. E. Arratia, *Microfluid. Nanofluid.* **14**, 885 406
 (2013). 407
 [36] J. J. Magda, C. S. Lee, and S. J. Muller, and R. G. Larson, 408
Macromolecules **26**, 1696 (1993). **5** 409
 [37] L. F. Moody, *Trans. ASME* **66**, 671 (1944). 410
 [38] Y. Jun and V. Steinberg, *Phys. Rev. Lett.* **102**, 124503 411
 (2009). 412
 [39] F. C. Cheong, B. J. Krishnatreya, and D. G. Grier, *Opt.* 413
Express **18**, 13563 (2010). 414
 [40] P. F. Salipante, C. A. E. Little, and S. D. Hudson, *Phys. Rev.* 415
Fluids **2**, 033302 (2017). 416
 417

418	[41] M. Alves, F. Pinho, and P. Oliveira, <i>J. Fluid Mech.</i> 97 , 207	[44] D. Samanta, Y. Dubief, M. Holzner, C. Schäfer, A. N. Morozov, C. Wagner, and B. Hof, <i>Proc. Natl. Acad. Sci. U.S.A.</i> 110 , 10557 (2013).	424
419	(2001).		425
420	[42] B. Thomases, M. Shelley, and J. Thiffeault, <i>Physica (Amsterdam)</i> 240D , 1602 (2011).	[45] G. H. Choueiri, J. M. Lopez, and B. Hof, <i>Phys. Rev. Lett.</i> 120 , 124501 (2018).	426
421			427
422	[43] P. Pakdel and G. H. McKinley, <i>Phys. Rev. Lett.</i> 77 , 2459		428
423	(1996).		429